Determination of dark energy by the Einstein Telescope: Comparing with CMB, BAO, and SNIa observations

W. Zhao,[1] C. Van Den Broeck,[2] D. Baskaran,[1] and T. G. F. Li[2]

[1]*School of Physics and Astronomy, Cardiff University, Cardiff, CF24 3AA, United Kingdom*
[2]*Nikhef – National Institute for Subatomic Physics, Science Park 105, 1098 XG Amsterdam, The Netherlands*

A design study is currently in progress for a third-generation gravitational-wave (GW) detector called the Einstein Telescope (ET). An important kind of source for ET will be the inspiral and merger of binary neutron stars up to $z \sim 2$. If binary neutron star mergers are the progenitors of short-hard γ-ray bursts, then some fraction of them will be seen both electromagnetically and through GW, so that the luminosity distance and the redshift of the source can be determined separately. An important property of these "standard sirens" is that they are *self-calibrating:* the luminosity distance can be inferred directly from the GW signal, with no need for a cosmic distance ladder. Thus, standard sirens will provide a powerful independent check of the ΛCDM model. In previous work, estimates were made of how well ET would be able to measure a subset of the cosmological parameters (such as the dark energy parameter w_0) it will have access to, assuming that the others had been determined to great accuracy by alternative means. Here we perform a more careful analysis by explicitly using the potential Planck cosmic microwave background data as prior information for these other parameters. We find that ET will be able to constrain w_0 and w_a with accuracies $\Delta w_0 = 0.099$ and $\Delta w_a = 0.302$, respectively. These results are compared with projected accuracies for the JDEM baryon acoustic oscillations project and the SNAP type Ia supernovae observations.

I. INTRODUCTION

In the past decade, various observations, including type Ia supernovae (SNIa) [1], the temperature and polarization anisotropies power spectrum of the cosmic microwave background (CMB) radiation [2], the baryon acoustic oscillations (BAO) peak in the distribution of Sloan Digital Sky Survey luminous red galaxies [3], and weak gravitational lensing [4], have all suggested that the present Universe is undergoing an accelerated expansion. A possible explanation would be the presence of a fluid called dark energy, which should have positive density but negative pressure (for a review, see [5]). Understanding the physical character of dark energy, assuming it exists, is one of the main challenges of modern cosmology. A key question is then how well we will be able to differentiate between various dark energy models by measuring the dark energy equation of state (EOS) and its time evolution.

Currently, among the main methods to determine the dark energy EOS are observations of SNIa, CMB, and large-scale structure. The capabilities of these methods will be improved significantly in the near future [6,7]. However, we note that all these methods are based on the observations of various electromagnetic waves. In addition to these electromagnetic methods, the observation of gravitational waves (GW) will provide a new technique, where gravitational-wave sources, in particular, inspiraling and merging compact binaries, can be considered as standard candles, or *standard sirens* [8]. In the case of ground-based detectors, the idea is to use binaries composed of two neutron stars (BNS), or a neutron star and a black hole (NSBH). These are hypothesized to be at the origin of short-hard γ-ray bursts (shGRBs). In many cases it is possible to identify the host galaxy of a shGRB and determine its redshift. From the gravitational-wave signal itself one would be able to measure the luminosity distance in an absolute way, without having to rely on a cosmic distance ladder: standard sirens are *self-calibrating*.

The use of GW standard sirens to measure the Hubble constant with a network of advanced ground-based detectors has been studied by Nissanke *et al.* [9], and with LISA (using extreme mass ratio inspirals) by MacLeod and Hogan [10]. Supermassive binary black holes may be useful to study dark energy with LISA [11–16]; more generally, they can constrain alternative theories of cosmology and gravity [17–20]. Observations of BNS events with the Big Bang Observer would also allow for dark energy studies [21].

Currently a third-generation ground-based observatory called Einstein Telescope (ET) is undergoing a design study [22]. The latter would be able to see BNS inspirals up to redshifts of $z \sim 2$ and NSBH events up to $z \sim 8$, corresponding to millions of sources over the course of several years, some fraction of which will have a detectable electromagnetic counterpart (e.g., a shGRB). Sathyaprakash *et al.* have investigated how well cosmological parameters could be determined with ET assuming 1000 "useful" sources [23]. Among the parameters which ET will have access to are

$$(H_0, \Omega_m, \Omega_k, w_0, w_a), \qquad (1)$$

where H_0 is the Hubble parameter at the current epoch, Ω_m the density of matter by the critical density, Ω_k a parameter related to spatial curvature, and w_0 and w_a parameters determining the dark energy EOS and its time evolution (see below for more precise definitions). ET will not be able to arrive at a completely independent measurement of all these parameters at once. In [23] it was assumed that, e.g., all parameters except w_0 had been measured by other means (electromagnetic or GW) and could be assumed known with arbitrary accuracy for all practical purposes. Here we continue this study in more depth, with a focus on the dark energy parameters w_0 and w_a. Instead of assuming the other parameters to be exactly known, we will use the predicted CMB prior from Planck. CMB measurements give accurate values for H_0, Ω_m, Ω_k, but have large uncertainties in w_0 and w_a. Heuristically, imposing this prior effectively "fixes" the values of H_0, Ω_m, Ω_k. To measure w_0, w_a with GW standard sirens is then an important check of the values obtained through electromagnetic means.

The outline of the paper is as follows. In Sec. II, we recall the basics of using short-hard γ-ray bursts as standard sirens in potential ET-GW observations. We then discuss the determination of the dark energy parameters by the ET-GW method alone, after which we impose the Planck CMB prior. In Sec. III, we discuss the capabilities of the JDEM BAO project and of the SNAP SNIa project, and a comparison as well as the potential combination with the ET-GW method is given. In Sec. IV we conclude with a summary of our main results.

II. SHORT-HARD γ-RAY BURSTS AS A KIND OF STANDARD SIREN

A. The expanding Universe and the dark energy

We will work with the Friedmann-Lemaître-Robertson-Walker universes, which are described by

$$ds^2 = -dt^2 + a^2(t)\left\{\frac{dr^2}{1 - kr^2} + r^2 d\theta^2 + r^2\sin^2\theta d\phi^2\right\}, \qquad (2)$$

where t is the cosmic time, and (r, θ, ϕ) are the comoving spatial coordinates. The parameter $k = 0, 1, -1$ describes the flat, closed, and open universe, respectively. The evolution of the scale factor $a(t)$ depends on the matter and energy contents of the Universe. Within general relativity, the equations governing this evolution are

$$\left(\frac{\dot{a}}{a}\right)^2 \equiv H^2 = \frac{8\pi G\rho_{\rm tot}}{3} - \frac{k}{a^2},$$
$$\frac{\ddot{a}}{a} = -\frac{4\pi G}{3}(\rho_{\rm tot} + 3p_{\rm tot}), \qquad (3)$$

where $\rho_{\rm tot}$ and $p_{\rm tot}$ are the total energy density and pressure in the Universe, and H is the Hubble parameter. Since in

this paper we are mainly interested in the later stages of the evolution of the Universe, where the radiation component can be ignored, we only take into account baryonic matter, dark matter, and dark energy. The baryon and dark matter are both modeled as pressureless dust. We will assume that the EOS of a dark energy component is responsible for the recent expansion of the Universe, which should be determined by observations. In this paper, we shall adopt a phenomenological form for the equation-of-state parameter w as a function of redshift z:

$$w(z) \equiv p_{\rm de}/\rho_{\rm de} = w_0 + w_a(1 - a) + \mathcal{O}[(1 - a)^2]$$
$$\simeq w_0 + w_a \frac{z}{1 + z}. \qquad (4)$$

This is the so-called Chevallier-Polarski-Linder form, [24] which has been adopted by many authors, including the DETF (Dark Energy Task Force) group [6]. In the present epoch where $z \simeq 0$, we have $w \simeq w_0$. w_a describes the evolution of w to next-to-leading order in $(1 - a)$. Since we are mostly interested in the later stages of the Universe's evolution, higher order terms will be ignored.

The evolution of dark energy is determined by the energy conservation equation $\dot{\rho}_{\rm de} + 3H(\rho_{\rm de} + p_{\rm de}) = 0$. By using the EOS of dark energy, Eq. (4), we find that

$$\rho_{\rm de} = \rho_{\rm de,0} \times E(z), \qquad (5)$$

where $\rho_{\rm de,0}$ is the value of $\rho_{\rm de}$ at $z = 0$, and

$$E(z) \equiv (1 + z)^{3(1+w_0+w_a)}e^{-3w_a z/(1+z)}. \qquad (6)$$

Using Eq. (3), the Hubble parameter H then becomes

$$H(z) = H_0[\Omega_m(1 + z)^3 + \Omega_k(1 + z)^2 + (1 - \Omega_m$$
$$- \Omega_k)E(z)]^{1/2}. \qquad (7)$$

In this expression, $\Omega_m \equiv 8\pi G\rho_{m,0}/3H_0^2$ is the density of matter (baryon as well as dark matter) relative to the critical density, and $\Omega_k \equiv -k/H_0^2$ is the contribution of the spatial curvature. H_0 is the Hubble parameter at the present epoch. Throughout this paper, we shall adopt a fiducial cosmological model with the following values for the parameters [2]:

$$w_0 = -1, \qquad w_a = 0, \qquad \Omega_b h_0^2 = 0.02267,$$
$$\Omega_c h_0^2 = 0.1131, \qquad \Omega_k = 0, \qquad h_0 = 0.705, \qquad (8)$$

where $h_0 = H_0/(100 \text{ km s}^{-1} \text{ Mpc}^{-1})$. The other parameters are obtained as $\Omega_m = \Omega_b + \Omega_c = 0.2736$, $\Omega_{de} = 1 - \Omega_m - \Omega_k = 0.7264$. In Sec. II D, the CMB prior for the dark energy determination will be discussed, where the perturbation parameters A_s and n_s (the amplitude and spectral index of primordial density perturbations, respectively) and the reionization parameter τ (the optical depth of reionization) are also needed. In our fiducial model, we take these to be [2]

$$A_s = 2.445 \times 10^{-9}, \quad n_s = 0.96, \quad \tau = 0.084. \qquad (9)$$

To conclude this subsection, we state the expression for the luminosity distance d_L of the astrophysical sources as a function of redshift z (see, e.g., [6]):

$$d_L(z) = (1 + z) \begin{cases} |k|^{-1/2} \sin\left[|k|^{1/2} \int_0^z \frac{dz'}{H(z')}\right] & (\Omega_k < 0), \\ \int_0^z \frac{dz'}{H(z')} & (\Omega_k = 0), \\ |k|^{-1/2} \sinh\left[|k|^{1/2} \int_0^z \frac{dz'}{H(z')}\right] & (\Omega_k > 0), \end{cases}$$

(10)

where $|k|^{1/2} \equiv H_0\sqrt{|\Omega_k|}$. This formula will be used frequently in the subsequent discussion.

B. Short-hard γ-ray bursts and gravitational waves

Current observational studies of dark energy strongly rely on *standard candles*, i.e., sources for which the intrinsic luminosity is assumed to be known within a certain tolerance so that they can be used to determine luminosity distance. A widely used standard candle is the type Ia supernova (SNIa) [1,25]. The intrinsic luminosity of distant SNIa needs to be calibrated by comparison with different kinds of closer-by sources, leading to a "cosmic distance ladder." This is not the case with GW standard sirens. As pointed out by Schutz, the chirping GW signals from inspiraling compact binary stars (neutron stars and black holes) can provide an absolute measure of distance, with no dependence on other sources [8]. The GW amplitude depends on the so-called chirp mass (a certain combination of the component masses) and the luminosity distance. However, the chirp mass can already be measured from the signal's phasing, so that the luminosity distance can be extracted from the amplitude.

Before discussing standard sirens in more detail, let us first recall some basic facts about the gravitational radiation emitted by inspiraling compact binaries. Gravitational waves are described by a second rank tensor $h_{\alpha\beta}$, which, in the so-called transverse-traceless gauge, has only two independent components h_+ and $h_\times$, $h_{xx} = -h_{yy} = h_+$, $h_{xy} = h_{yx} = h_\times$, all other components being zero. A detector measures only a certain linear combination of the two components, called the response $h(t)$, which is given by (see, e.g., [26])

$$h(t) = F_+(\theta, \phi, \psi)h_+(t) + F_\times(\theta, \phi, \psi)h_\times(t), \quad (11)$$

where F_+ and $F_\times$ are the detector antenna pattern functions, ψ is the polarization angle, and (θ, ϕ) are angles describing the location of the source on the sky, relative to the detector. In general these angles are time-dependent. In the case of Einstein Telescope, binary neutron star signals can be in band for hours, but almost all of the signal-to-noise ratio will be accumulated in the final minutes of the inspiral process. With LISA, Doppler modulation due to the orbital motion, as well as spin precession, will allow for accurate determination of the angular parameters (see, e.g.,

[27] and references therein), but this is unlikely to happen for BNS (or NSBH) signals in ET with Doppler modulation due to the Earth's rotation. Nevertheless, some improvement in parameter estimation can be expected, which for simplicity we do not take into account here. In the sequel, (θ, ϕ, ψ) will be considered constant.

Consider a coalescing binary at a luminosity distance d_L, with component masses m_1 and m_2. Write $M = m_1 + m_2$ for the total mass and $\eta = m_1 m_2/M^2$ for the symmetric mass ratio, and define the "chirp mass" as $\mathcal{M}_c = M\eta^{3/5}$. For sources at cosmological distances, what enters the waveform is the *observed* chirp mass, which differs from the *physical* chirp mass by a factor $(1 + z)$: $\mathcal{M}_{c,\text{obs}} = (1 + z)\mathcal{M}_{c,\text{phys}}$. Below, $\mathcal{M}_c$ will always refer to the observed quantity. To leading order in amplitude, the GW polarizations are

$$h_+(t) = 2\mathcal{M}_c^{5/3}d_L^{-1}(1 + \cos^2(\iota))\omega^{2/3}(t_0 - t)$$
$$\times \cos[2\Phi(t_0 - t; M, \eta) + \Phi_0], \quad (12)$$

$$h_\times(t) = 4\mathcal{M}_c^{5/3}d_L^{-1}\cos(\iota)\omega^{2/3}(t_0 - t)$$
$$\times \sin[2\Phi(t_0 - t; M, \eta) + \Phi_0], \quad (13)$$

where ι is the angle of inclination of the binary's orbital angular momentum with the line of sight, $\omega(t_0 - t)$ the angular velocity of the equivalent one-body system around the binary's center of mass, and $\Phi(t_0 - t; M, \eta)$ the corresponding orbital phase. The parameters t_0 and Φ_0 are constants giving the epoch of merger and the orbital phase of the binary at that epoch, respectively. The phase Φ has been computed perturbatively in the so-called post-Newtonian formalism (see [28] and references therein). Since we will mostly be concerned with binary neutron stars, spin will not be important, in which case the phase is known up to 3.5PN in the usual notation [29], and this is what we will use here.

During the inspiral, the change in orbital frequency over a single period is negligible, and it is possible to apply a stationary phase approximation to compute the Fourier transform $\mathcal{H}(f)$ of the time domain waveform $h(t)$. One has

$$\mathcal{H}(f) = \mathcal{A}f^{-7/6}\exp[i(2\pi f t_0 - \pi/4 + 2\psi(f/2)$$
$$- \varphi_{(2,0)})], \quad (14)$$

where the Fourier amplitude $\mathcal{A}$ is given by

$$\mathcal{A} = \frac{1}{d_L}\sqrt{F_+^2(1 + \cos^2(\iota))^2 + F_\times^2 4\cos^2(\iota)}$$
$$\times \sqrt{\frac{5\pi}{96}}\pi^{-7/6}\mathcal{M}_c^{5/6}. \quad (15)$$

The functions ψ and $\varphi_{(2,0)}$ are

$$\psi(f) = -\psi_0 + \frac{3}{256\eta}\sum_{i=0}^{7}\psi_i(2\pi Mf)^{i/3}, \quad (16)$$

$$\varphi_{(2,0)} = \tan^{-1}\left(-\frac{2\cos(\iota)F_\times}{(1 + \cos^2(\iota))F_+}\right). \quad (17)$$

The parameters ψ_i can be found in [26]. $\mathcal{H}(f)$ is taken to be zero outside a certain frequency range. The upper cutoff frequency is dictated by the last stable orbit, which marks the end of the inspiral regime and the onset of the final merger. We will assume that this occurs when the radiation frequency reaches $f_{upper} = 2f_{LSO}$, with $f_{LSO} = 1/(6^{3/2}2\pi M_{obs})$ the orbital frequency at the last stable orbit, and $M_{obs} = (1 + z)M_{phys}$ the observed total mass.

In this paper we shall focus on the observation of GW sources by the Einstein Telescope, a third-generation ground-based gravitational-wave detector. Although the basic design of ET is still under discussion, one possibility is to have three interferometers with 60° opening angles and 10 km arm lengths, arranged in an equilateral triangle [22]. The corresponding antenna pattern functions are

$$F_+^{(1)}(\theta, \phi, \psi) = \frac{\sqrt{3}}{2}\left[\frac{1}{2}(1 + \cos^2(\theta))\cos(2\phi)\cos(2\psi)\right.$$
$$\left. - \cos(\theta)\sin(2\phi)\sin(2\psi)\right],$$

$$F_\times^{(1)}(\theta, \phi, \psi) = \frac{\sqrt{3}}{2}\left[\frac{1}{2}(1 + \cos^2(\theta))\cos(2\phi)\sin(2\psi)\right.$$
$$\left. + \cos(\theta)\sin(2\phi)\cos(2\psi)\right],$$

$$F_{+,\times}^{(2)}(\theta, \phi, \psi) = F_{+,\times}^{(1)}(\theta, \phi + 2\pi/3, \psi),$$

$$F_{+,\times}^{(3)}(\theta, \phi, \psi) = F_{+,\times}^{(1)}(\theta, \phi + 4\pi/3, \psi). \quad (18)$$

The performance of a GW detector is characterized by the one-side noise *power spectral density* $S_h(f)$ (PSD), which plays an important role in the signal analysis. We take the noise PSD of ET to be [30,31]

$$S_h(f) = S_0\left[x^{p_1} + a_1 x^{p_2} + a_2\frac{1 + b_1 x + b_2 x^2 + b_3 x^3 + b_4 x^4 + b_5 x^5 + b_6 x^6}{1 + c_1 x + c_2 x^2 + c_3 x^3 + c_4 x^4}\right], \quad (19)$$

where $x \equiv f/f_0$ with $f_0 = 200$ Hz, and $S_0 = 1.449 \times 10^{-52}$ Hz^{-1}. The other parameters are as follows:

$$p_1 = -4.05, \quad p_2 = -0.69, \quad a_1 = 185.62,$$
$$a_2 = 232.56, \quad b_1 = 31.18, \quad b_2 = -64.72,$$
$$b_3 = 52.24, \quad b_4 = -42.16, \quad b_5 = 10.17,$$
$$b_6 = 11.53 \quad c_1 = 13.58, \quad c_2 = -36.46,$$
$$c_3 = 18.56, \quad c_4 = 27.43. \quad (20)$$

For data analysis proposes, the noise PSD is assumed to be essentially infinite below a certain lower cutoff frequency f_{lower} (see the review [26]). For ET we take this to be $f_{lower} = 1$ Hz.

The waveforms in Eq. (14) depend on the seven free parameters $(\ln\mathcal{M}_c, \ln\eta, t_0, \Phi_0, \cos(\iota), \psi, \ln d_L)$; note that for "useful" events the sky position will be known. In order to deal with the parameter estimation, throughout this paper, we employ the Fisher matrix approach [32]. Comparing with the Markov chain Monte Carlo analysis, the Fisher information matrix analysis is simple and accurate enough to estimate the detection abilities of the future experiments. In the case of a single interferometer A ($A = 1, 2, 3$), the Fisher matrix is given by

$$\Lambda_{ij}^{(A)} = \langle\mathcal{H}_i^{(A)}, \mathcal{H}_j^{(A)}\rangle, \quad \mathcal{H}_i^{(A)} = \partial\mathcal{H}^{(A)}(f)/\partial p_i, \quad (21)$$

where $\mathcal{H}^{(A)}$ is the output of interferometer A, and the p_i denote the free parameters to be estimated, which are

$$(\ln\mathcal{M}_c, \ln\eta, t_0, \Phi_0, \cos(\iota), \psi, \ln d_L). \quad (22)$$

The angular brackets denote the scalar product, which, for any two functions $a(t)$ and $b(t)$ is defined as

$$\langle a, b\rangle = 4\int_{f_{lower}}^{f_{upper}}\frac{\tilde{a}(f)\tilde{b}^*(f) + \tilde{a}^*(f)\tilde{b}(f)}{2}\frac{df}{S_h(f)}, \quad (23)$$

where $\tilde{a}$ and $\tilde{b}$ are the Fourier transforms of the functions $a(t)$ and $b(t)$. The Fisher matrix for the combination of the three independent interferometers is then

$$\Lambda_{ij} = \sum_{A=1}^{3}\Lambda_{ij}^{(A)}. \quad (24)$$

The inner product also allows us to write the signal-to-noise ratios $\rho^{(A)}$, $A = 1, 2, 3$ in a compact way:

$$\rho^{(A)} = \sqrt{\langle\mathcal{H}^{(A)}, \mathcal{H}^{(A)}\rangle}. \quad (25)$$

The combined signal-to-noise ratio for the network of the three independent interferometers is then

$$\rho = \left[\sum_{A=1}^{3}(\rho^{(A)})^2\right]^{1/2}. \quad (26)$$

In this paper, we shall focus on the estimation of the parameter $\ln d_L$. The 1-σ observational error, σ_o, can be estimated from the Fisher matrix Λ_{ij}. An important point is that shGRBs are believed to be beamed: the γ radiation is emitted in a narrow cone more or less perpendicular to the plane of the inspiral. We will take the total beaming angle to be at most 40° [33] (corresponding to $\iota \leq 20°$). It will be assumed that shGRBs are produced by the mergers of the neutron star binaries. For definiteness we take them to

have component masses of $(1.4, 1.4)M_{\text{sun}}$. We will consider 1000 sources up to a redshift of $z = 2$, which is where the angle-averaged signal-to-noise ratio approximately reaches the value 8 for sources with $\iota < 20°$.

Before continuing, we mention that coalescing binaries composed of a neutron star and a black hole could also cause shGRBs [33]. For a fixed distance, a NSBH event will have a larger signal-to-noise ratio than a BNS event, leading to an improved measurement of $\ln d_L$. The intrinsic event rates for NSBH are quite uncertain, but they are expected to be considerably lower than for BNS [34]; on the other hand, NSBH events will be visible to ET out to redshifts of $z \sim 4$ [23]. It is likely that the inclusion of NSBH would have a noticeable beneficial effect on the determination of cosmological parameters, especially if the black holes have spin, but this we leave for future studies.

For a given event, distance measurements will be subject to two kinds of uncertainties: the instrumental error σ_o which can be estimated using a Fisher matrix as discussed above, and an additional error σ_l due to the effects of weak lensing. As in previous work [23] we assume the contribution to the distance error from weak lensing to satisfy $\sigma_l = 0.05z$. Thus, the total uncertainty on $\Delta \ln d_L$ is taken to be

$$\Delta \ln d_L = \sqrt{\sigma_o^2 + \sigma_l^2}. \qquad (27)$$

In the next subsection we discuss how the information from multiple GW standard sirens can be combined to compute the expected measurement uncertainties on cosmological parameters.

C. Gravitational-wave standard sirens

Now let us turn to the determination of the cosmological parameters, including dark energy parameters, by GW standard sirens. For each shGRB source, the luminosity distance d_L is measured from the GW observation, and the redshift z can be obtained from the electromagnetic counterpart. Thus, the $d_L - z$ relation can be employed to constrain various cosmological parameters. For the cosmological model introduced in Sec. II A, we consider five free parameters $(w_0, w_a, \Omega_m, \Omega_k, h_0)$ which can be constrained by GW standard sirens. We note that the value of Ω_{de} (the relative energy density of the dark energy component) is determined by the quantities Ω_m and Ω_k through $\Omega_{de} \equiv 1 - \Omega_m - \Omega_k$.

In order to estimate the errors on these parameters, we study a Fisher matrix F_{ij}^{GW} for a collection of inspiral events:

$$F_{ij}^{\text{GW}} = \sum_k \frac{\partial_i (\ln d_L(k)) \partial_j (\ln d_L(k))}{(\Delta \ln d_L(k))^2}, \qquad (28)$$

where the indices i and j run from 1 to 5, denoting the free parameters $(w_0, w_a, \Omega_m, \Omega_k, h_0)$. Equation (10) gives the

expression for d_L, and the partial derivatives with respect to the parameters are evaluated at the parameter values corresponding to the fiducial cosmological model of Sec. II A. The uncertainty $\Delta \ln d_L$ is calculated by using Eq. (27). The index $k = 1, 2, \ldots,$ labels the event at $(z_k, \hat{\gamma}_k)$, where the vector $\hat{\gamma}$ stands for the angles $(\theta, \phi, \iota, \psi)$. Here we should mention that, in (28), we have ignored the photometric redshift errors and the possible errors generated by the peculiar velocities of the sources relative to the Hubble flow [35]. Given that the majority of our sources will be at $z > 0.4$, we do not expect the latter to make much difference to our main results.

Since d_L is independent of $\hat{\gamma}$, this Fisher matrix can be rewritten as

$$F_{ij}^{\text{GW}} = \sum_{z_k} \partial_i (\ln d_L(z_k)) \partial_j (\ln d_L(z_k)) \left\{ \sum_{\hat{\gamma}_k} \frac{1}{(\Delta \ln d_L(z_k, \hat{\gamma}_k))^2} \right\}. \qquad (29)$$

When the number of events is large, the sum over events in (29) can be replaced by an integral, so that we obtain

$$F_{ij}^{\text{GW}} = \int_0^2 \partial_i (\ln d_L) \partial_j (\ln d_L) f(z) A(z) dz, \qquad (30)$$

where $f(z)$ is the number distribution of the GW sources over redshift z. $A(z)$ is the average of $1/(\Delta \ln d_L(z, \hat{\gamma}))^2$ over the angles $(\theta, \phi, \iota, \psi)$ with the constraint $\iota < 20°$:

$$A(z) \equiv \left\langle \frac{1}{(\Delta \ln d_L(z, \hat{\gamma}))^2} \right\rangle_{\hat{\gamma}; \iota < 20°}. \qquad (31)$$

In order to calculate the averaged quantity $A(z)$, we used a Monte Carlo sampling with 10 000 choices of $\hat{\gamma}$ for a given z, where z ranges from 0 to 2 in steps of 0.1. The results are indicated in Fig. 1 by the red dots. We find that these points
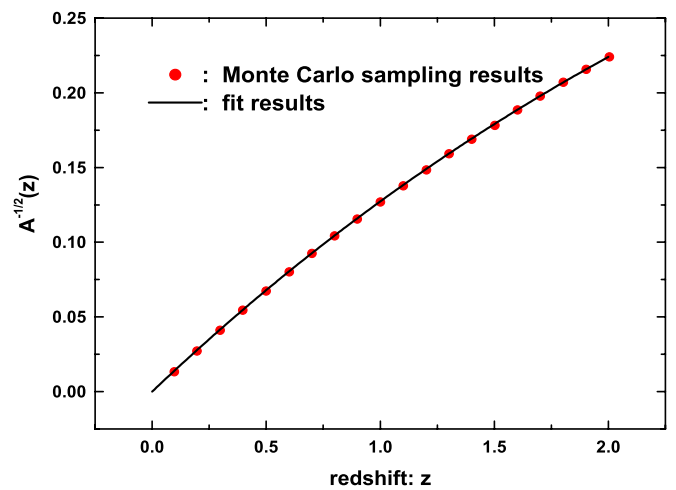

FIG. 1 (color online). The averaged quantity $A^{-1/2}(z)$ [defined in (31)] as a function of redshift z. The red dots denote the results based on the Monte Carlo sampling, and the solid line denotes the fit results.
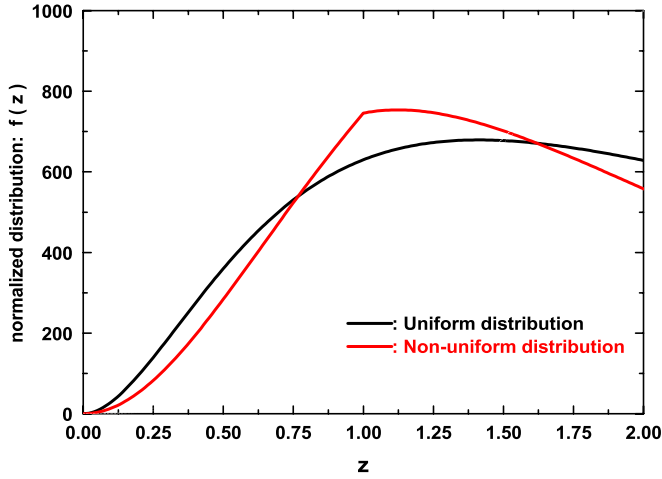
FIG. 2 (color online). The normalized distribution of the GW sources.

can be fit very accurately by a simple relation (see the black solid line in Fig. 1):

$$A^{-1/2}(z) = 0.1449z - 0.0118z^2 + 0.0012z^3, \quad (32)$$

which is used in our subsequent calculation.

In (30), the upper integration limit $z = 2$ is the redshift at which the angle-averaged signal-to-noise ratio is approximately 8 [23]. In our fiducial model with $\Omega_k = 0$, the number distribution $f(z)$ is given by

$$f(z) = \frac{4\pi\mathcal{N}r(z)d_C^2(z)}{H(z)(1+z)}, \quad (33)$$

where d_C is the comoving distance, which is defined as $d_C(z) \equiv \int_0^z 1/H(z')dz'$. The function $r(z)$ describes the time evolution of the burst rate, and the constant $\mathcal{N}$ (the number of the sources per comoving volume at redshift $z = 0$ over the observation period) is fixed by requiring the total number of the sources $N_{GW} = \int_0^2 f(z)dz$. The expected total number of inspirals per year within the horizon of ET is ~several $\times 10^5$ for neutron star binaries. If, as suspected, neutron star binaries are progenitors of shGRBs [33], it might be possible to make a coincident detection of a significant subset of the events in the GW and electromagnetic windows, which can then be considered as standard sirens. As we have mentioned, shGRBs are believed to be beamed with small beaming angle, so only a small fraction of the total number of neutron star binaries are

expected to be observed as shGRBs. Following [23], we assume that about 1000 events (~ 10^{-3} of the total number of binary coalescences) will be observed in both windows, i.e., $N_{GW} = 1000$ throughout this paper.

Since the time evolution of the source rate is as yet unclear, in this paper we shall consider two different forms for the function $r(z)$. In the first case we assume that the sources are distributed uniformly, i.e., with constant comoving number density throughout the redshift range $0 \leq z \leq 2$ (hereafter we will refer to this as the uniform distribution). In this case we have $r(z) = 1$, which is what was assumed in the previous work [23]. In the other case, we take $r(z)$ to be the following function: $r(z) = (1 + 2z)$ for $z \leq 1$, $r(z) = (15 - 3z)/4$ for $1 < z < 5$, and $z = 0$ for $z \geq 5$. This approximate fit to the rate evolution is suggested in [36]. Hereafter, we shall call this the nonuniform distribution. In Fig. 2, we plot the distribution function f as a function of redshift z in the two cases. Note that in the case with nonuniform distribution, the sources are a little more concentrated at $z = 1$. In what follows we will find out how this affects the uncertainties on the cosmological parameters.

Using the definition (30), we can calculate the Fisher matrix F_{ij}^{GW} for the following two cases: *a. GW events with uniform distribution; b. GW events with nonuniform distribution.* The results are listed in Tables I and II.

From the Fisher matrices, we can calculate the 1-σ uncertainties on the parameters, which are $\Delta p_i = \sqrt{(F^{GW})_{ii}^{-1}}$. For the case with uniform distribution, by using the results in Table I, we find that

$$\Delta w_0 = 2.62, \qquad \Delta w_a = 9.53, \qquad \Delta\Omega_m = 0.815,$$
$$\Delta\Omega_k = 2.03, \qquad \Delta h_0 = 1.20 \times 10^{-2}. \quad (34)$$

We plot the two-dimensional uncertainty contour of the parameters w_0 and w_a in Fig. 3 (blue curve, i.e., line 2, in the left panel). Unfortunately, we find that the error bars on the parameters are all fairly large, especially for the dark energy parameters w_0 and w_a. This is caused by the strong degeneracy between (w_0, w_a) and the other parameters $(\Omega_m, \Omega_k, h_0)$, especially (Ω_m, Ω_k). To illustrate this, let us do the following calculation. First we fix the values of the parameters $(\Omega_m, \Omega_k, h_0)$ to be their fiducial values, and only consider (w_0, w_a) as free parameters. By using the results in Table I, we obtain

TABLE I. GW Fisher matrix in the case with uniform distribution.

	w_0	w_a	Ω_m	Ω_k	h_0
w_0	$0.273\,681 \times 10^4$	$0.433\,681 \times 10^3$	$0.753\,068 \times 10^4$	$0.261\,216 \times 10^4$	$0.221\,885 \times 10^5$
w_a	$0.433\,681 \times 10^3$	$0.753\,710 \times 10^2$	$0.128\,638 \times 10^4$	$0.406\,152 \times 10^3$	$0.317\,462 \times 10^4$
Ω_m	$0.753\,068 \times 10^4$	$0.128\,638 \times 10^4$	$0.221\,212 \times 10^5$	$0.704\,345 \times 10^4$	$0.571\,447 \times 10^5$
Ω_k	$0.261\,216 \times 10^4$	$0.406\,152 \times 10^3$	$0.704\,345 \times 10^4$	$0.251\,558 \times 10^4$	$0.213\,013 \times 10^5$
h_0	$0.221\,885 \times 10^5$	$0.317\,462 \times 10^4$	$0.571\,447 \times 10^5$	$0.213\,013 \times 10^5$	$0.216\,280 \times 10^6$

TABLE II.   GW Fisher matrix in the case with nonuniform distribution.

	w_0	w_a	Ω_m	Ω_k	h_0
w_0	$0.256\,794 \times 10^4$	$0.427\,648 \times 10^3$	$0.731\,269 \times 10^4$	$0.244\,368 \times 10^4$	$0.194\,634 \times 10^5$
w_a	$0.427\,648 \times 10^3$	$0.762\,633 \times 10^2$	$0.129\,200 \times 10^4$	$0.399\,934 \times 10^3$	$0.303\,753 \times 10^4$
Ω_m	$0.731\,269 \times 10^4$	$0.129\,200 \times 10^4$	$0.219\,941 \times 10^5$	$0.682\,599 \times 10^4$	$0.529\,628 \times 10^5$
Ω_k	$0.244\,368 \times 10^4$	$0.399\,934 \times 10^3$	$0.682\,599 \times 10^4$	$0.234\,666 \times 10^4$	$0.186\,267 \times 10^5$
h_0	$0.194\,634 \times 10^5$	$0.303\,753 \times 10^4$	$0.529\,628 \times 10^5$	$0.186\,267 \times 10^5$	$0.162\,814 \times 10^6$

$$\Delta w_0 = 0.064, \qquad \Delta w_a = 0.388. \qquad (35)$$

We find that the values of Δw_0 and Δw_a become much smaller in this case. The two-dimensional uncertainty contour of w_0 and w_a is also plotted in Fig. 3 (black curve, i.e., line 1, in the left panel). This figure shows that there is correlation between the parameters w_0 and w_a. Recall that a goal of the dark energy programs is to test whether dark energy arises from a simple cosmological constant, ($w_0 = -1$, $w_a = 0$). For a given data set we can do better (as far as excluding the cosmological constant model is concerned) than simply quoting the values of Δw_0 and Δw_a. This is because the effect of dark energy is generally not best constrained at $z = 0$. For the phenomenological form of the EOS of the dark energy $w(z) = w_0 + w_a z/(1 + z)$, the constraint on $w(z)$ varies with the redshift z. So, similar to [6], we can define the best pivot redshift, denoted as z_p, where the uncertainty in $w(z)$ equals the uncertainty in a model that assumes $w_a = 0$. In this paper, we denote the EOS at this best pivot redshift as $w_p \equiv w(z_p)$. The best pivot redshift z_p can be calculated by $z_p = -1/(1 + \frac{\Delta w_a}{\rho \Delta w_0})$, where ρ is the correlation coefficient of w_0 and w_a. The value of Δw_p is calculated by

$\Delta w_p = \Delta w_0 \sqrt{1 - \rho^2}$. In this case (two free parameters), the results for z_p and Δw_p are

$$z_p = 0.188, \qquad \Delta w_p = 0.019. \qquad (36)$$

The value of Δw_p as well as that of Δw_a are commonly used to describe the detection ability of the experiments [6].

On the other hand, we can also fix the values of the parameters (w_0, w_a) to be their fiducial values, and only consider (Ω_m, Ω_k, h_0) as free parameters. By using the results in Table I, we obtain

$$\Delta\Omega_m = 0.021, \qquad \Delta\Omega_k = 0.087,$$
$$\Delta h_0 = 5.48 \times 10^{-3}. \qquad (37)$$

Again we find that the values of these errors, especially the values of $\Delta\Omega_m$ and $\Delta\Omega_k$, are much smaller that those in Eq. (34). These results show that the GW standard sirens can constrain the dark energy parameters rather well, on condition that we can break the strong degeneracy between the parameters (w_0, w_a) and the parameters (Ω_m, Ω_k, h_0). In the next subsection, we will find that this can be realized if we consider the CMB observations as a prior.
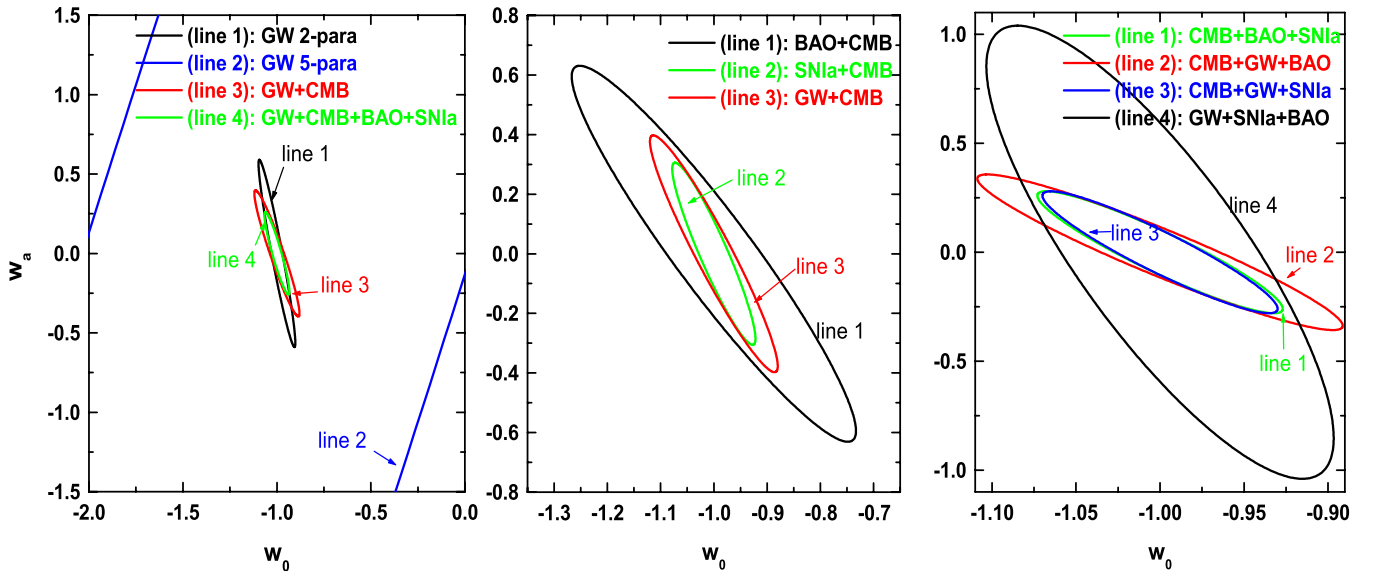

FIG. 3 (color online).   The two-dimensional uncertainty contours of the dark energy parameters w_0 and w_a in the case with uniform distribution.
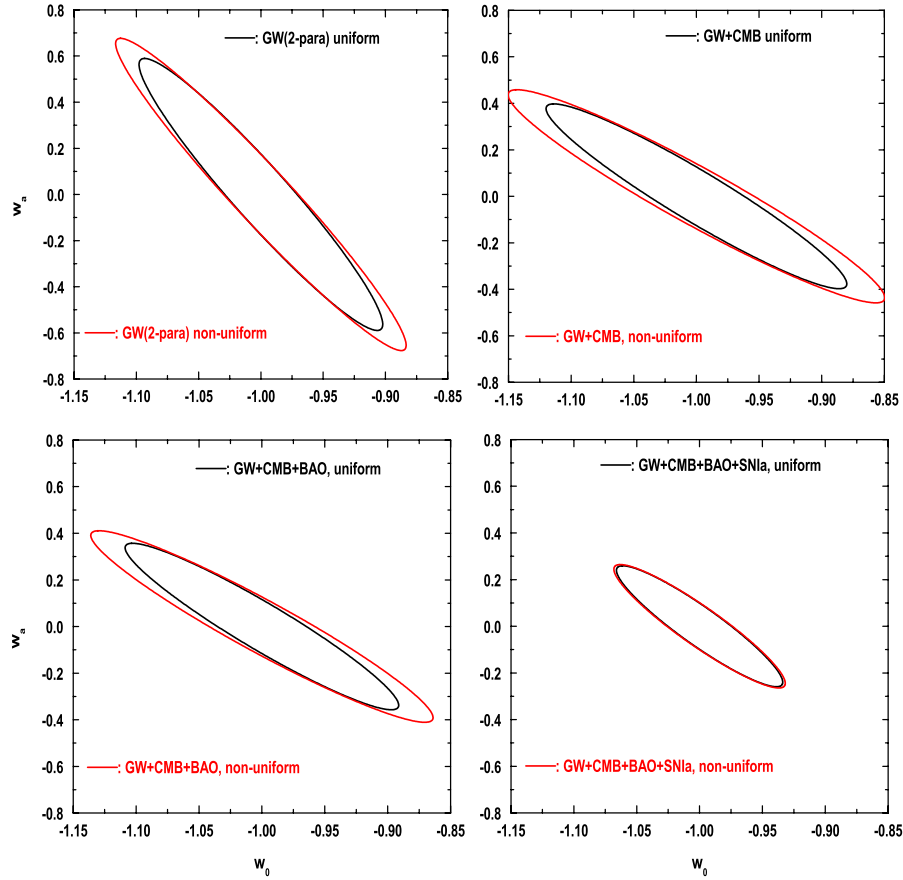
FIG. 4 (color online).   The two-dimensional uncertainty contours for the dark energy parameters w_0 and w_a, in the different cases.

To conclude this subsection we discuss the determination of the dark energy parameters (w_0, w_a) by ET observations in two cases considered in this paper. By using the results in Tables I and II, we calculate the errors of the two parameters (the other parameters are fixed at their fiducial values). The two-dimensional uncertainty contours are shown in Fig. 4 (upper left panel). This figure shows that the errors of the parameters are a little larger for the nonuniform distribution than those in the corresponding case with the uniform distribution. This is because the sources in the nonuniform distribution are a little more concentrated at the redshift $z = 1$. Hence the number of the sources in the high redshift and the low redshift regions is smaller, making it more difficult to constrain the dark energy's evolution. So, in addition to the number of the sources, the redshift distribution of the sources also plays a crucial role for the detection of dark energy. The results listed in (35) constitute the optimistic case among the cases we have considered. On the other hand, it is helpful to list the results in the case with nonuniform distribution, which are

$$\Delta w_0 = 0.077, \qquad \Delta w_a = 0.445. \qquad (38)$$

We find that these uncertainties are a little larger than those in (35). We can also calculate the values of z_p and Δw_p for this case, which are

$$z_p = 0.200, \qquad \Delta w_p = 0.020. \qquad (39)$$

The value of Δw_p is also a little larger than that in the case with uniform distribution.

D. Planck CMB prior

As will be clear from the discussion above, the ability of GW sources to constrain dark energy depends strongly on how well the background parameters Ω_m and Ω_k can be measured beforehand. Indeed, if one tries to determine these background parameters as well as the dark energy parameters together using GW sources, the values of Δw_0 and Δw_a become very large, and the constraints on dark energy become meaningless. Hence we should consider another observational method which can determine these background parameters through a prior observation. As we shall see, this is also necessary for the other ways used to study dark energy—BAO and SNIa—so that it does not diminish the value of having self-calibrating standard sirens: GW observations will provide us with an important independent check.

Observations of the cosmic microwave background temperature and polarization anisotropies are always used as the required prior. The WMAP satellite has already given fairly good results for the CMB TT (temperature-temperature autocorrelation) and TE (temperature-polarization cross

TABLE III.   CMB Fisher matrix.

	w_0	w_a	Ω_m	Ω_k	h_0
w_0	$0.414\,303 \times 10^5$	$0.115\,085 \times 10^5$	$0.287\,229 \times 10^6$	$-0.678\,690 \times 10^6$	$0.339\,923 \times 10^6$
w_a	$0.115\,085 \times 10^5$	$0.320\,204 \times 10^4$	$0.797\,415 \times 10^5$	$-0.190\,373 \times 10^6$	$0.943\,498 \times 10^5$
Ω_m	$0.287\,229 \times 10^6$	$0.797\,415 \times 10^5$	$0.219\,854 \times 10^7$	$-0.465\,663 \times 10^7$	$0.251\,813 \times 10^7$
Ω_k	$-0.678\,690 \times 10^6$	$-0.190\,373 \times 10^6$	$-0.465\,663 \times 10^7$	$0.136\,912 \times 10^8$	$-0.548\,091 \times 10^7$
h_0	$0.339\,923 \times 10^6$	$0.943\,498 \times 10^5$	$0.251\,813 \times 10^7$	$-0.548\,091 \times 10^7$	$0.291\,587 \times 10^7$

correlation) power spectra in the multipole range $\ell < 800$. The background parameters (Ω_m, Ω_k) have already been well determined by 7-year WMAP observations; for example, the constraint on the curvature is $-0.0133 < \Omega_k < 0.0084$ (95% C.L.) [2]. These constraints are expected to be greatly improved by the Planck observations [37], which will give good data on the CMB TT and TE power spectra up to $\ell \sim 2000$. In addition, Planck is also expected to observe the EE (electric type polarization) power spectrum. In this subsection, we shall consider the potential CMB observations by the Planck satellite. For the noise power spectra of Planck, we consider the instrumental noises at three frequency channels: at 100 GHz, 143 GHz, and 217 GHz. For the reduced foreground radiations (including dust and synchrotron), we assume that the reduced factor $\sigma^{\mathrm{fg}} = 0.1$, i.e., 10% residual foregrounds are considered as the noises. The total noise power spectra N_ℓ^{TT} and N_ℓ^{EE} of the Planck satellite can be found in [38]. Note that in this paper we assume 4 sky (28 months) survey.

In order to estimate the constraints on the cosmological parameters, we shall again use the Fisher information matrix technique. The Fisher matrix is calculated by [39]

$$F_{ij}^{\mathrm{CMB}} = \sum_{\ell=2}^{\ell_{\max}} \sum_{XX',YY'} \frac{\partial C_\ell^{XX'}}{\partial p_i} \mathrm{Cov}^{-1}(D_\ell^{XX'}, D_\ell^{YY'}) \frac{\partial C_\ell^{YY'}}{\partial p_j},$$

(40)

where p_i are the cosmological parameters to be evaluated. $C_\ell^{XX'}$ are the CMB power spectra and $D_\ell^{XX'}$ are their estimates. Cov^{-1} is the inverse of the covariance matrix. The nonvanishing components of the covariance matrix are given by

$$\mathrm{Cov}(D_\ell^{XX}, D_\ell^{XX}) = \frac{2}{(2\ell+1)f_{\mathrm{sky}}}(C_\ell^{XX} + N_\ell^{XX})^2 (X = T, E),$$

$$\mathrm{Cov}(D_\ell^{TE}, D_\ell^{TE}) = \frac{1}{(2\ell+1)f_{\mathrm{sky}}}[(C_\ell^{TE})^2 + (C_\ell^{TT} + N_\ell^{TT}) \times (C_\ell^{EE} + N_\ell^{EE})],$$

$$\mathrm{Cov}(D_\ell^{TT}, D_\ell^{EE}) = \frac{2}{(2\ell+1)f_{\mathrm{sky}}}(C_\ell^{TE})^2,$$

$$\mathrm{Cov}(D_\ell^{TT}, D_\ell^{TE}) = \frac{2}{(2\ell+1)f_{\mathrm{sky}}}C_\ell^{TE}(C_\ell^{TT} + N_\ell^{TT}),$$

$$\mathrm{Cov}(D_\ell^{EE}, D_\ell^{TE}) = \frac{2}{(2\ell+1)f_{\mathrm{sky}}}C_\ell^{TE}(C_\ell^{EE} + N_\ell^{EE}).$$

Note that in the calculation we have adopted $\ell_{\max} = 2000$, and the sky-cut factor $f_{\mathrm{sky}} = 0.65$ suggested by the Planck Bluebook [37].

The CMB power spectra $C_\ell^{XX'}$ depend on all the cosmological parameters, including the background parameters and the perturbation parameters. In the calculation, we first build the Fisher matrix for the full nine parameters $(w_0, w_a, \Omega_b h_0^2, \Omega_c h_0^2, \Omega_k, n_s, A_s, h_0, \tau)$. In order to obtain the constraint on the parameter Ω_m, we change the full Fisher matrix to the new one of the nine parameters $(w_0, w_a, \Omega_m, \Omega_c h_0^2, \Omega_k, n_s, A_s, h_0, \tau)$, where $\Omega_m = (\Omega_b h_0^2 + \Omega_c h_0^2)/h_0^2$ has been used. In order to directly compare and combine with the Fisher matrix of GW method, we marginalize the new nine-parameter Fisher matrix to the one with five parameters $(w_0, w_a, \Omega_m, \Omega_k, h_0)$. The results are shown in Table III. The errors of the parameters are given by $\Delta p_i = \sqrt{(F^{\mathrm{CMB}})_{ii}^{-1}}$. By using the Fisher matrix in Table III, we obtain

$$\Delta w_0 = 0.411,$$
$$\Delta w_a = 0.517,$$
$$\Delta \Omega_m = 8.88 \times 10^{-2}, \qquad (41)$$
$$\Delta \Omega_k = 2.27 \times 10^{-3},$$
$$\Delta h_0 = 0.115.$$

This result shows that Planck alone can give quite tight constraints on Ω_m and Ω_k, which is just complementary with the GW method. However, CMB observations alone cannot constrain the parameters w_0 and w_a, which is because that the CMB power spectra are only sensitive to the physics in the early Universe at $z \sim 1100$, where dark energy is totally subdominant.

We now investigate the combination of CMB and GW methods. In order to do this, we define a new Fisher matrix, which is the sum of F_{ij}^{GW} and F_{ij}^{CMB}. By using this new Fisher matrix, we obtain

$$\Delta w_0 = 0.079,$$
$$\Delta w_a = 0.261,$$
$$\Delta \Omega_m = 5.14 \times 10^{-3}, \qquad (42)$$
$$\Delta \Omega_k = 6.66 \times 10^{-4},$$
$$\Delta h_0 = 5.96 \times 10^{-3},$$

for the uniform distribution case. We find that the values of Δw_0 and Δw_a are fairly close to those in Eq. (35), where we have only considered the GW observations but assumed the backgrounds parameters Ω_m, Ω_k and h_0 are fixed. These results show that taking the CMB observation as a prior is nearly equivalent to fixing the parameters Ω_m, Ω_k and h_0. The two-dimensional uncertainty contour of the parameters w_0 and w_a is shown in Fig. 3 (red lines, i.e., line 3, in the left panel and the middle panel). We can also calculate the best pivot redshift z_p and the value of Δw_p, which are

$$z_p = 0.401, \qquad \Delta w_p = 0.025. \qquad (43)$$

By the same method, we also obtain the results in the nonuniform distribution case. The two-dimensional uncertainty contour of w_0 and w_a is shown in Fig. 4 (upper-right panel). In this case, the results are

$$\Delta w_0 = 0.099,$$
$$\Delta w_a = 0.302,$$
$$\Delta \Omega_m = 7.30 \times 10^{-3}, \qquad (44)$$
$$\Delta \Omega_k = 6.70 \times 10^{-4},$$
$$\Delta h_0 = 8.99 \times 10^{-3}.$$

The best pivot redshift z_p and the uncertainty Δw_p are

$$z_p = 0.454, \qquad \Delta w_p = 0.030. \qquad (45)$$

Again as expected, we find that the values are larger than the corresponding values in the uniform distribution case.

III. DETECTION OF DARK ENERGY BY BAO AND SNIA OBSERVATIONS, AND THE COMPARISON WITH ET-GW OBSERVATIONS

In the above we found that by combining the potential Planck CMB observation with ET-GW observations, one can get fairly tight constraints on the dark energy parameters w_0 and w_a. In this section we discuss the detection abilities of the other two probes: BAO and SNIa. Currently these two methods play the crucial role for the determination of the dark energy component. In the near future, the detection abilities of these two methods are expected to be significantly improved; in this section a detailed discussion is given. All three probes, BAO, SNIa and GW, constrain the EOS of dark energy by probing the large-scale background geometry of the Universe (different from the weak gravitational lensing method [40]), so a fair comparison can be made, as we shall do here.

A. Detection of dark energy by potential BAO observations

The BAO method relies on the distribution of baryonic matter to infer the redshift-distance relation.

The characteristic scale length of structure which can be accurately determined from the CMB is used as a standard rod. By measuring the angular size of this characteristic scale-length as a function of redshift, the effect of dark energy can be inferred. The BAO method can constrain the dark energy by two observable quantities $\ln(H(z))$ and $\ln(d_A(z))$, where $H(z)$ is the binned Hubble parameter and $d_A(z)$ is comoving angular diameter distance, which is related to the luminosity distance by $d_A = d_L/(1 + z)$. Similar to the quantity d_L, these two observables only depend on the cosmological parameters w_0, w_a, Ω_m, Ω_k and h_0, which will be considered as the parameters determined by the observations.

In order to investigate the constraints on the cosmological parameters, we build the following Fisher information matrix [6]:

$$F_{ij}^{\text{BAO}} = \sum_k \frac{\partial \ln(H(z_k))}{\partial p_i} \frac{\partial \ln(H(z_k))}{\partial p_j} \left(\frac{1}{\sigma_{\ln(H(z_i))}}\right)^2$$
$$+ \frac{\partial \ln(d_A(z_k))}{\partial p_i} \frac{\partial \ln(d_A(z_k))}{\partial p_j} \left(\frac{1}{\sigma_{\ln(d_A(z_i))}}\right)^2. \quad (46)$$

Again the index k denotes the observables, which are binned into several redshift bins. p_i denotes the cosmological parameters. $\sigma_{\ln(H(z))}$ and $\sigma_{\ln(d_A(z))}$ are the errors (including the observational errors and the systematic errors) of the observables $\ln(H(z))$ and $\ln(d_A(z))$, respectively. In order to study the detection ability of the BAO method, we shall consider the potential observations of a typical project, the final JDEM (Joint Dark Energy Mission) project [6], which is expected to survey $10\,000\text{deg}^2$ in the redshift range $z \in (0.5, 2)$. In the calculation, we bin the observables $\ln(H(z))$ and $\ln(d_A(z))$ into 10 redshift bins, i.e., $\Delta z = 0.15$ for each bin. The calculation of the theoretical values of these quantities are straightforward. For the errors of these observable data, we use the fitting formulae derived in [41] [see also Eq. (4.8) in [6]].

The results of the Fisher information matrix are shown in Table IV. To begin with we consider a simple case with only two free parameters (w_0, w_a). We assume that the other parameters (Ω_m, Ω_k, h_0) are fixed to their fiducial values. By using the Fisher matrix in Table IV, we obtain the uncertainties of the free parameters:

$$\Delta w_0 = 0.087, \qquad \Delta w_a = 0.346, \qquad z_p = 0.323,$$
$$\Delta w_p = 0.023. \qquad (47)$$

However, if we try to constrain all five parameters by BAO observations, the uncertainties of the parameters will become fairly large. For instance, the uncertainties of w_0 and w_a become $\Delta w_0 = 0.850$ and $\Delta w_a = 3.611$, respectively, which are much larger than those in (47). Similarly to the discussion in Sec. II D, we can consider

TABLE IV.   BAO Fisher matrix.

	w_0	w_a	Ω_m	Ω_k	h_0
w_0	$0.193\,253 \times 10^4$	$0.471\,352 \times 10^3$	$0.865\,506 \times 10^4$	$0.288\,000 \times 10^4$	$0.125\,880 \times 10^5$
w_a	$0.471\,352 \times 10^3$	$0.123\,299 \times 10^3$	$0.234\,243 \times 10^4$	$0.788\,613 \times 10^3$	$0.309\,758 \times 10^4$
Ω_m	$0.865\,506 \times 10^4$	$0.234\,243 \times 10^4$	$0.457\,760 \times 10^5$	$0.153\,244 \times 10^5$	$0.579\,934 \times 10^5$
Ω_k	$0.288\,000 \times 10^4$	$0.788\,613 \times 10^3$	$0.153\,244 \times 10^5$	$0.541\,597 \times 10^4$	$0.190\,452 \times 10^5$
h_0	$0.125\,880 \times 10^5$	$0.309\,758 \times 10^4$	$0.579\,934 \times 10^5$	$0.190\,452 \times 10^5$	$0.834\,616 \times 10^5$

the combination of the BAO observation and the Planck CMB prior. By analogous steps we obtain the results

$$\Delta w_0 = 0.176,$$
$$\Delta w_a = 0.415,$$
$$\Delta \Omega_m = 2.01 \times 10^{-2}, \qquad (48)$$
$$\Delta \Omega_k = 6.40 \times 10^{-4},$$
$$\Delta h_0 = 2.57 \times 10^{-2}.$$

The best pivot redshift and the value of Δw_p are

$$z_p = 0.664, \qquad \Delta w_p = 0.059. \qquad (49)$$

B. Detection of dark energy by potential SNIa observations

Now, let us turn to discuss the detection of dark energy parameters by the SNIa probe. Type Ia supernovae serve as a standard candle of (approximately) known luminosity. The redshift of supernova can be obtained by studying its spectral lines. Thus the redshift-distance relation can be gotten from SNIa surveys. Now, SNIa observed from various experiments have been used successfully to deduce the acceleration of the Universe after $z = 1$ [1,42]. In the near future, observations of SNIa are expected to be significantly improved, so that they will continue to serve as one of the most important methods for the determination of dark energy.

The observables for SNIa data are the apparent magnitudes m, which can be corrected to behave as standard candles with absolute magnitude M with $m = M + \mu(z)$. The function $\mu(z)$ for the measured redshift is

$$\mu(z) = 5\log_{10}(d_L(z)) + 25, \qquad (50)$$

where d_L is the luminosity distance. In this paper, we shall consider SNIa observations by the future SNAP (Supernova/Acceleration Probe) project [43]. As suggested by the SNAP group, we consider 300 low redshift supernovae, uniformly distributed over $z \in (0.03, 0.08)$. The error bar on the magnitude is assumed to be $\sigma_m = 0.15$ mag. In addition, 2000 high redshift supernovae in the range $z \in (0.1, 1.7)$ are considered. The expected redshift distribution of these sources can be found in the SNAP white book (the middle red curve in Fig. 9 of [43]). We bin these 2000 sources into 10 redshift bins in the range $z \in (0.1, 1.7)$. The total errors of the observables $\sigma(z)$ can be estimated as follows [43,44]:

$$\sigma = \sqrt{\sigma_1^2 + \sigma_2^2}, \qquad (51)$$

where $\sigma_1 = 0.15 \, \text{mag}/\sqrt{N}$ (N is the total number of supernovae in each bin) is the intrinsic random Gaussian error, and $\sigma_2 = 0.02 \, \text{mag}(1 + z)/2.7$ is the error due to the astrophysical systematics.

Thus, we can build a Fisher information matrix, which is

$$F_{ij}^{\text{SN}} = \sum_k \frac{\partial \mu(z_k)}{\partial p_i} \frac{\partial \mu(z_k)}{\partial p_j} \left(\frac{1}{\sigma(z_k)}\right)^2. \qquad (52)$$

The results are shown in Table V. The errors of the cosmological parameters are estimated by $\Delta p_i = \sqrt{(F^{\text{SN}})_{ii}^{-1}}$. Similar to Sec. III A, we first discuss the simplest case with two free parameters (w_0, w_a). The results are

$$\Delta w_0 = 0.054, \qquad \Delta w_a = 0.302, \qquad z_p = 0.211,$$
$$\Delta w_p = 0.012. \qquad (53)$$

To constrain all five cosmological parameters, we consider the combination of SNIa and the Planck CMB prior to

TABLE V.   SNIa Fisher matrix.

	w_0	w_a	Ω_m	Ω_k	h_0
w_0	$0.703\,955 \times 10^4$	$0.122\,773 \times 10^4$	$0.207\,309 \times 10^5$	$0.669\,019 \times 10^4$	$0.522\,067 \times 10^5$
w_a	$0.122\,773 \times 10^4$	$0.225\,085 \times 10^3$	$0.377\,761 \times 10^4$	$0.115\,185 \times 10^4$	$0.849\,589 \times 10^4$
Ω_m	$0.207\,309 \times 10^5$	$0.377\,761 \times 10^4$	$0.636\,028 \times 10^5$	$0.194\,262 \times 10^5$	$0.146\,902 \times 10^6$
Ω_k	$0.669\,019 \times 10^4$	$0.115\,185 \times 10^4$	$0.194\,262 \times 10^5$	$0.639\,862 \times 10^4$	$0.498\,026 \times 10^5$
h_0	$0.522\,067 \times 10^5$	$0.849\,589 \times 10^4$	$0.146\,902 \times 10^6$	$0.498\,026 \times 10^5$	$0.491\,151 \times 10^6$

decouple the degeneracy between (w_0, w_a) and the other parameters. The errors of the parameters are

$$\Delta w_0 = 0.051,$$
$$\Delta w_a = 0.201,$$
$$\Delta \Omega_m = 3.49 \times 10^{-3}, \qquad (54)$$
$$\Delta \Omega_k = 6.52 \times 10^{-4},$$
$$\Delta h_0 = 3.39 \times 10^{-3}.$$

We find that the values of Δw_0 and Δw_a in (54) are close to those in (53). The best pivot redshift and the value of Δw_p are also obtained

$$z_p = 0.313, \qquad \Delta w_p = 0.019. \qquad (55)$$

C. Comparison with the ET-GW observations

Now let us compare the detection abilities of various probes: GW, BAO and SNIa. First we consider the simplest case, where only dark energy parameters (w_0, w_a) are considered. The errors of the parameters are given in (47) for BAO, and in (53) for SNIa. We find that the values of Δw_0, Δw_a and Δw_p are all smaller for the SNIa probe. This shows that, comparing with the JDEM BAO project, the SNAP SNIa project is expected to give a tighter constraint on the dark energy. For the ET-GW project, in Sec. II C, we have considered two cases. For the uniform distribution case, the results are given in (35) and (36). On the other hand, if the nonuniform distribution case is considered, the results are shown in (38) and (39). Comparing with these results, we conclude that, in both cases, the detection ability of ET-GW method is stronger than that of the JDEM BAO project, but weaker than that of the SNAP SNIa project. This is mainly because the number of the GW standard sirens (~ 1000 as we have assumed) is smaller than that of the SNIa standard candles (~ 2000 at high redshift). In order to clearly show this, let us consider another case for ET-GW method, where we assume that 2000 sources with nonuniform distribution will be observed. We then obtain $\Delta w_0 = 0.054$, $\Delta w_a = 0.315$ and $\Delta w_p = 0.014$, which comes close to the projected uncertainties of the SNAP SNIa project given by (53). We note that the relative error bars of the SNIa in Eq. (51) are larger than those of GW sources in (32), especially at low redshifts. However, we find that this disadvantage of the SNIa method is overcome by the assumed 300 low redshift SNIa in $z \in (0.03, 0.08)$.

We can also compare the results of these three probes, when considering the full 5 cosmological parameters and adopting the Planck CMB prior. In Fig. 3 (middle panel), we plot the two-dimensional uncertainty contours of the parameters (w_0, w_a), where for the ET-GW method we have considered the case with uniform distribution. Similarly, we find that the red curve (GW + CMB) is

only a little looser than the green one (SNIa + CMB), but much tighter than the black one (BAO + CMB). In Fig. 3 (right panel), we plot the results of the two-dimensional uncertainty contours for the four combinations (CMB + BAO + SNIa, CMB + GW + BAO, CMB + GW + SNIa, GW + SNIa + BAO). We find that the first three combinations have similar results. However, the constraint on the dark energy parameters is much looser for combination of GW + SNIa + BAO, where the Planck CMB probe is absent. This panel shows that the CMB prior indeed plays a crucial role in the detection of dark energy.

Let us now combine all the four probes to constrain the cosmological parameters, including the dark energy parameters. If we consider the uniform distribution for the GW sources, we obtain the constraints on the dark energy parameters

$$\Delta w_0 = 0.044, \qquad \Delta w_a = 0.171,$$
$$z_p = 0.308, \qquad \Delta w_p = 0.017. \qquad (56)$$

This is the best constraint what we could expect to obtain. If we consider the case with nonuniform distribution for the GW sources, the constraints slightly loosen to

$$\Delta w_0 = 0.045, \qquad \Delta w_a = 0.174,$$
$$z_p = 0.313, \qquad \Delta w_p = 0.017. \qquad (57)$$

In Fig. 4 (lower-right panel), we plot the two-dimensional uncertainty contours of the parameters (w_0, w_a) for both cases. We find that the two curves are very close to each other; the relative weight of the GW probe is not very high for the combined methods.

Finally, we would like to know how much the ET-GW probe can contribute in constraining all the five cosmological parameters $(w_0, w_a, \Omega_m, \Omega_k, h_0)$. In order to do so, we first calculate the constraints on the parameters by the combination of CMB + BAO + SNIa. We obtain

$$\Delta w_0 = 0.048, \qquad \Delta w_a = 0.184,$$
$$\Delta \Omega_m = 3.46 \times 10^{-3}, \qquad \Delta \Omega_k = 5.91 \times 10^{-4},$$
$$\Delta h_0 = 3.36 \times 10^{-3}. \qquad (58)$$

If we then add the contribution of the ET-GW probe with nonuniform distribution (the uniform distribution case gives the very close results), the results become

$$\Delta w_0 = 0.045, \qquad \Delta w_a = 0.174,$$
$$\Delta \Omega_m = 3.39 \times 10^{-3}, \qquad \Delta \Omega_k = 5.83 \times 10^{-4},$$
$$\Delta h_0 = 3.20 \times 10^{-3}. \qquad (59)$$

In this case we find that, due to the contribution of ET-GW probe, Δw_0 is decreased by a 6.3% and Δw_a by 5.5%. In Fig. 5 we plot the two-dimensional uncertainty contours of
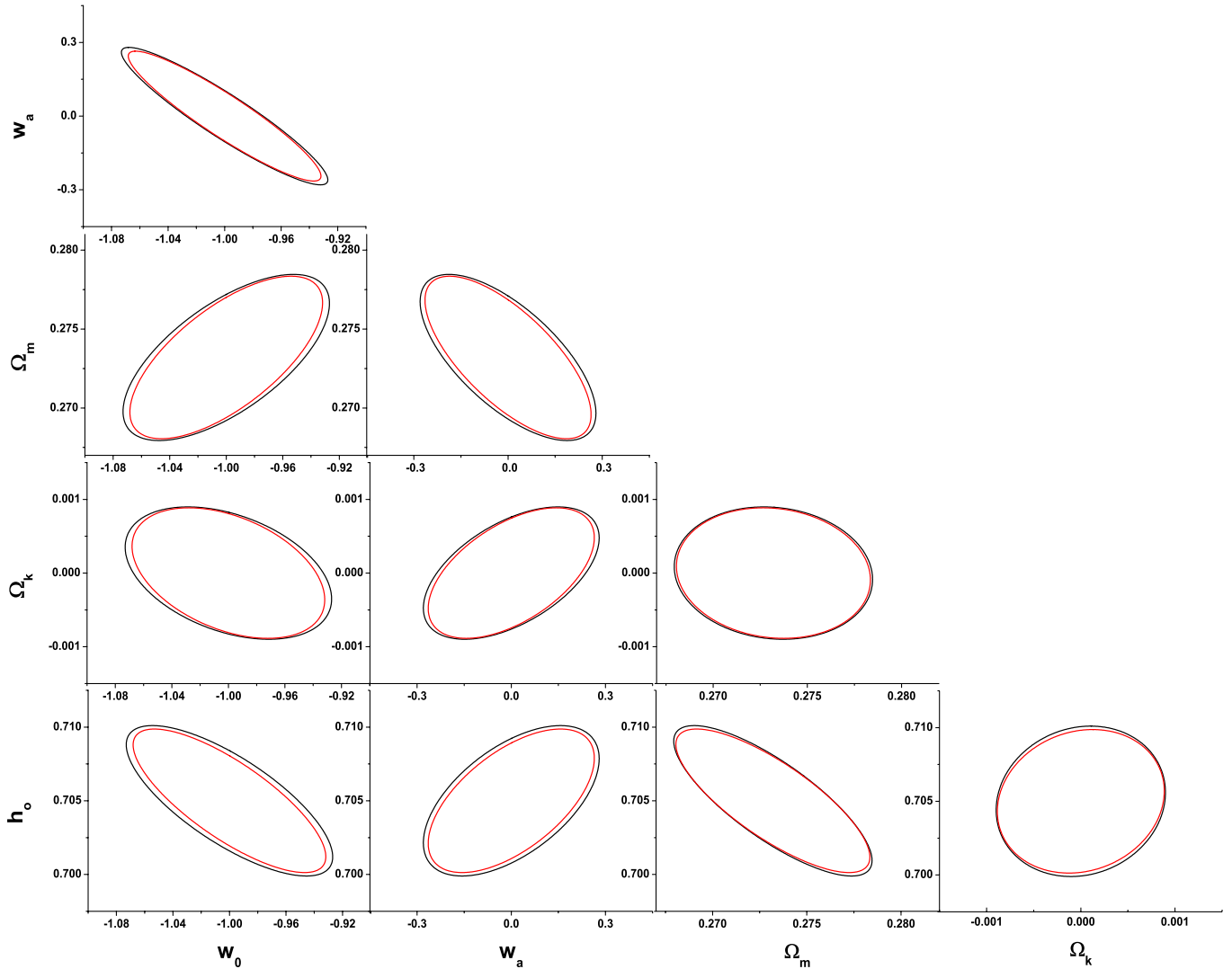
FIG. 5 (color online).   The two-dimensional uncertainty contours of the cosmological parameters. The black (larger) curves denote the results of CMB + BAO + SNIa, and the red (smaller) curves denote the results of CMB + BAO + SNIa + GW. Here, we have assumed the GW with nonuniform distribution (The case with uniform distribution gives the nearly overlapped results).

the free parameters (w_0, w_a, Ω_m, Ω_k, h_0) for both combinations.

IV. CONCLUSION

If short-hard γ-ray bursts are produced by the mergers of neutron star binaries, the luminosity distances d_L of the sources can be determined by the Einstein Telescope gravitational-wave detector in the redshift range $z < 2$. The redshifts z of the sources can be determined with great accuracy through their electromagnetic counterparts. Thus it will be possible to use shGRBs as "standard sirens" to study the dark energy component in the Universe by determining the EOS and its time evolution.

When calculating the uncertainties in the determination of d_L by the ET observations, we assumed that the γ-ray

emission is confined to a cone with an opening angle as large as 40° [33], corresponding to inclination angles $\iota < 20°$. In order to study the effect of the redshift distribution of the sources, we considered two different kinds of distributions: one in which sources are distributed uniformly in comoving volume, and a nonuniform distribution as in [36]. We found that, by taking into account the Planck CMB prior, the errors on the dark energy parameters are expected to be $\Delta w_0 = 0.079$ and $\Delta w_a = 0.261$ in the uniform distribution case, which is close to the detection ability of the SNAP Type Ia Supernovae project. Even in the "pessimistic" case with nonuniform distribution of the sources, the errors are $\Delta w_0 = 0.099$ and $\Delta w_a = 0.302$, which is weaker than the detection ability of the SNAP Type Ia Supernova project, but stronger than that of the JDEM baryon acoustic oscillation project. We also found

that, with the combination of the future CMB(Planck) + BAO(JDEM) + SNIa(SNAP) projects, the contribution of these kinds of standard sirens can decrease the error of w_0 by ~6.3% and that of w_a by ~5.5%. Thus, the kinds of self-calibrating GW standard sirens accessible to the Einstein Telescope would provide an excellent probe of the dark energy component.

Finally, it is important to mention that, in addition to GW, CMB, BAO, and SNIa methods, there are a number of other probes, including cosmic weak lensing, galaxy clustering, and so on, which can also be used to detect the dark energy component in the Universe (see [6,45] for details). In practice, one should combine all the probes. However, in this paper, we have emphasized that using shGRBs as

''standard sirens'' constitutes an important complement to the general electromagnetic methods.

ACKNOWLEDGMENTS

[1] M. Kowalski *et al.*, Astrophys. J. **686**, 749 (2008); M. Hicken *et al.*, Astrophys. J **700**, 1097 (2009).

[2] E. Komatsu *et al.* (WMAP Collaboration), Astrophys. J. Suppl. Ser. **180**, 330 (2009); arXiv:1001.4538.

[3] D. J. Eisenstein *et al.* (SDSS Collaboration), Astrophys. J. **633**, 560 (2005); W. J. Percival *et al.*, Mon. Not. R. Astron. Soc. **381**, 1053 (2007); W. J. Percival *et al.*, Mon. Not. R. Astron. Soc. **401**, 2148 (2010).

[4] T. Schrabback *et al.*, arXiv:0911.0053; M. Kilbinger *et al.*, Astron. Astrophys. **497**, 677 (2009).

[5] E. J. Copeland, M. Sami, and S. Tsujikawa, Int. J. Mod. Phys. D **15**, 1753 (2006).

[6] A. Albrecht *et al.*, arXiv:astro-ph/0609591.

[7] A. Refregier *et al.*, arXiv:1001.0061; P. A. Abell *et al.* (LSST Science. Collaborations), arXiv:0912.0201.

[8] B. Schutz, Nature (London) **323**, 310 (1986).

[9] S. Nissanke, S. A. Hughes, D. E. Holz, N. Dalal, and J. L. Sievers, Astrophys. J. **725**, 496 (2010);

[10] C. L. MacLeod and C. J. Hogan, Phys. Rev. D **77**, 043512 (2008).

[11] D. E. Holz and S. A. Hughes, Astrophys. J **629**, 15 (2005).

[12] N. Dalal, D. E. Holz, S. A. Hughes, and B. Jain, Phys. Rev. D **74**, 063006 (2006).

[13] K. G. Arun, B. R. Iyer, B. S. Sathyaprakash, S. Sinha, and C. Van Den Broeck, Phys. Rev. D **76**, 104016 (2007); K. G. Arun, C. K. Mishra, C. Van Den Broeck, B. R. Iyer, B. S. Sathyaprakash, and S. Sinha, Classical Quantum Gravity **26**, 094021 (2009).

[14] C. Van Den Broeck, M. Trias, B. S. Sathyaprakash, and A. M. Sintes, Phys. Rev. D **81**, 124031 (2010).

[15] A. Stavridis, K. G. Arun, and C. M. Will, Phys. Rev. D **80**, 067501 (2009).

[16] S. Babak, J. R. Gair, A. Petiteau, and A. Sesana, arXiv:1011.2062.

[17] C. Deffayet and K. Menou, Astrophys. J **668**, L143 (2007).

[18] B. Kocsis, Z. Haimain, and K. Menou, Astrophys. J **684**, 870 (2008).

[19] E. Berti, A. Buonanno, and C. M. Will, Phys. Rev. D **71**, 084025 (2005); Classical Quantum Gravity **22**, S943 (2005).

[20] K. G. Arun and C. M. Will, Classical Quantum Gravity **26**, 155002 (2009).

[21] C. Cutler and D. E. Holz, Phys. Rev. D **80**, 104009 (2009).

[22] ''The Einstein Telescope Project,'' https://www.et-gw .eu/et/.

[23] B. S. Sathyaprakash, B. F. Schutz, and C. Van Den Broeck, Classical Quantum Gravity **27**, 215006 (2010).

[24] M. Chevallier and D. Polarski, Int. J. Mod. Phys. D **10**, 213 (2001); E. V. Linder, Phys. Rev. Lett. **90**, 091301 (2003).

[25] A. G. Riess *et al.*, Astron. J. **116**, 1009 (1998); S. Perlmutter *et al.*, Astrophys. J **517**, 565 (1999).

[26] B. S. Sathyaprakash and B. F. Schutz, Living Rev. Relativity **12**, 2 (2009).

[27] M. Trias and A. M. Sintes, Phys. Rev. D **77**, 024030 (2008).

[28] L. Blanchet, Living Rev. Relativity **5**, 3 (2002).

[29] T. Damour, P. Jaranowski, and G. Schäfer, Phys. Lett. B **513**, 147 (2001); Y. Itoh, T. Futamase, and H. Asada, Phys. Rev. D **63**, 064038 (2001); L. Blanchet, G. Faye, B. R. Iyer, and B. Joguet, Phys. Rev. D **65**, 061501(R) (2002); **71**, 129902(E) (2005); Y. Itoh and T. Futamase, Phys. Rev. D **68**, 121501(R) (2003); Y. Itoh, Phys. Rev. D **69**, 064018 (2004); L. Blanchet, T. Damour, and G. Esposito-Farèse, Phys. Rev. D **69**, 124007 (2004); L. Blanchet, T. Damour, G. Esposito-Farèse, and B. R. Iyer, Phys. Rev. Lett. **93**, 091101 (2004); Y. Itoh, Classical Quantum Gravity **21**, S529 (2004); L. Blanchet and B. R. Iyer, Phys. Rev. D **71**, 024004 (2005).

[30] A. Freise *et al.*, arXiv:0908.0353.

[31] This PSD corresponds to one possible design of ET; the same reference [30] also discusses alternatives.

[32] L. S. Finn, Phys. Rev. D **46**, 5236 (1992); L. S. Finn and D. F. Chernoff, Phys. Rev. D **47**, 2198 (1993).

[33] E. Nakar, Phys. Rep. **442**, 166 (2007).

[34] LIGO Scientific Collaboration and Virgo Collaboration, Classical Quantum Gravity **27**, 173001 (2010).

[35] B. Kocsis, Z. Frei, Z. Haiman, and K. Menou, Astrophys. J **637**, 27 (2006).

[36] R. Schneider, V. Ferrari, S. Matarrese, and S. F. Portegies Zwart, Mon. Not. R. Astron. Soc. **324**, 797 (2001).

[37] Planck Collaboration, arXiv:astro-ph/0604069.

[38] See e.g., W. Zhao, D. Baskaran, and L. P. Grishchuk, Phys. Rev. D **80**, 083005 (2009) (Appendix B).

[39] M. Tegmark, A. Taylor, and A. Heavens, Astrophys. J **480**, 22 (1997); M. Zaldarriaga, D. Spergel, and U. Seljak, Astrophys. J **488**, 1 (1997).

[40] M. Bartelmann and P. Schneider, Phys. Rep. **340**, 291 (2001); W. Hu and B. Jain, Phys. Rev. D **70**, 043009 (2004); D. Munshi, P. Valageas, L. Van Waerbeke, and A. Heavens, Phys. Rep. **462**, 67 (2008).

[41] C. Blake et al., Mon. Not. R. Astron. Soc. **365**, 255 (2006).

[42] M. Kowalski et al., Astrophys. J **686**, 749 (2008); M. Hicken et al., Astrophys. J **700**, 331 (2009).

[43] SNAP Collaboration, arXiv:astro-ph/0405232.

[44] E. V. Linder and D. Huterer, Phys. Rev. D **67**, 081303 (R) (2003).

[45] S. Wang, J. Khoury, Z. Haiman, and M. May, Phys. Rev. D **70**, 123008 (2004).